Synthesis of Nanocrystalline SiC via Sol–Gel Method: Effect of Low-Temperature Heat Treatment on Phase Formation and Nanostructures

Zahra Zalnezhad[1], Morteza Sasani Ghamsari[2]*, Hamid Heratizadeh[1]

[1]Faculty of Nuclear Physics and Engineering, Shahrood University of Technology, Shahrood, Iran
[2]Photonics and Quantum Technologies Research Institute, NSTRI, Tehran, Iran[1]
Email: msghamsari@yahoo.com

Abstract

Silicon carbide (SiC) is one of the most important silicon-based compounds, owing to its favorable physical, chemical, and biological properties, and is widely employed in various fields such as electronics, chemical industries, and quantum computing. Several methods have been reported for synthesizing SiC nanoparticles, including chemical vapor deposition (CVD), hydrothermal synthesis, carbothermal reduction, and sol–gel processing. Among these, the sol–gel method has attracted significant attention due to its high yield, process controllability, biocompatibility, accessibility of precursors, and ability to produce nanoparticles. In this study, SiC nanosized powders were synthesized through the sol–gel route combined with carbothermal reduction, using tetraethyl orthosilicate $(C_2H_5)_4SiO_4$ and sucrose $(C_{11}H_{22}O_{11})$ as the silicon and carbon sources, respectively. The silica/sucrose composite was subjected to carbothermal reduction under an argon atmosphere at a pressure of 10 mTorr in a vacuum furnace at 1350°C for 3 h. The structural properties of the synthesized SiC nanopowders were analyzed using X-ray diffraction (XRD), while their optical characteristics were investigated through FTIR, diffuse reflectance spectroscopy (DRS), and photoluminescence (PL). This work demonstrates a greener, lower-temperature route to phase-controlled SiC nanoparticles with optically active vacancy centers.

Keywords: *Silicon carbide nanoparticles, Sol–Gel, Carbothermal reduction*

[DOI: 10.22068/ijmse.4346]

---

[1] *Corresponding author: msghamsari@yahoo.com

1. Introduction

Silicon carbide (SiC), one of the earliest known semiconductors, has recently gained renewed attention due to its ability to function under extreme conditions such as high temperature, high power, high frequency, and strong radiation environments. It has also been extensively applied in advanced electronic, optoelectronic, and quantum technologies because of its capacity to generate single photons. SiC is a wide-bandgap semiconductor that exists in various polytypes, the most common of which are 4H, 6H, 15R, and 3C. The wide bandgap and remarkable optical emission features (such as donor–acceptor pairs and color centers) have broadened the optical applications of this material [1,2]. The existence of multiple polytypes further enables the design of devices adaptable to advanced environments and suitable for quantum photonic platforms [3]. In recent years, the presence of color centers—particularly silicon vacancies (V_{Si})—in the SiC lattice has established it as a promising platform for room-temperature single-photon emission and spin-based qubits. Unlike nitrogen-vacancy (NV) centers in diamond, SiC offers CMOS compatibility, paving the way for integration of quantum and classical technologies. However, the efficient synthesis of SiC nanoparticles with simultaneous control over particle size, phase purity, and quantum properties remains a significant challenge [4]. Several approaches have been developed for SiC nanostructure synthesis, such as carbothermal reduction [5], chemical vapor deposition (CVD) [6], direct carbonization of metallic silicon [7], high-energy mechanical milling [8], and sol–gel processing. Most of these methods, however, either require extremely high processing temperatures (above 2000°C) or involve toxic precursors such as HF and HNO_3, rendering the synthesis costly, hazardous, and environmentally undesirable [9]. Furthermore, specialized equipment or complex technology requirements in some methods elevate production costs and

[DOI: 10.22068/ijmse.4346]

often result in low efficiency and high impurity content. By contrast, the sol–gel method, an aqueous chemical process widely employed for the synthesis of inorganic and ceramic materials, has been broadly utilized in producing metal oxides, nanocoatings, aerogels, and nanocomposites. Starting from a metal precursor (commonly a metal alkoxide or salt), which largely determines the final structure, the sol–gel process proceeds through sequential steps: hydrolysis (formation of reactive groups), polymerization (formation of metal–oxide bonds, controlling particle size, surface area, and structural homogeneity), sol formation, gelation (stabilizing the final structure), drying (influencing porous or dense morphology), and thermal treatment (enhancing crystallinity). In recent years, sol–gel processing has emerged as a highly attractive method, offering high-purity products, molecular-level mixing, and favorable chemical reactivity [10]. This approach enables the synthesis of nanocrystallites smaller than 100 nm at relatively low temperatures (below 1500°C). For instance, Najafi et al. (2022) synthesized β-SiC at 1500°C by optimizing acidic pH conditions during the sol–gel process. When pH was below 4, the solution became more stable, and β-SiC nanoparticles as small as 10 nm were achieved; however, in the range pH = 4–7, the solution stability decreased, and particle size increased significantly. Nevertheless, the use of HF remained a limiting factor [11]. Similarly, Li et al. (2023) employed tetraethyl orthosilicate (TEOS) and phenolic resin as precursors, with oxalic acid (OA) and hexamethylenetetramine (HMTA) as catalysts [12]. Their findings revealed that OA primarily regulated the solution pH and influenced the hydrolysis of TEOS, while HMTA facilitated coagulation and gelation. Through this dual-catalyst system, SiC nanoparticles of ~60 nm were synthesized at 1500°C, though polytype control could not be achieved [12]. Zhang et al. successfully synthesized SiC nanoparticles using a carbon–SiO_2 mixture [13]. This approach significantly reduced particle size and enabled synthesis at much lower temperatures compared with the Acheson process, yielding β-SiC nanoparticles of ~30 nm at 1500°C, although particle agglomeration was observed. Other

[DOI: 10.22068/ijmse.4346]

methods, such as plasma pyrolysis by Garcia (2019) at 1700°C [14], carbothermal–mechanical synthesis by Chen (2021) at 1550°C [15], and CVD by Wang (2022) at 1580°C [16], not only required higher temperatures but also produced particles predominantly larger than 100 nm.

Although sol–gel synthesis provides advantages such as compositional uniformity and precise structural control, challenges remain. The most critical factor is the accurate adjustment of the precursor ratio between silica and the carbon source, as an imbalance can result in residual silica or free carbon, reducing the purity of the SiC phase. Moreover, complete conversion of the gel to SiC generally requires high temperatures (typically above 1400°C), which may promote excessive grain growth or the crystallization of unwanted phases. Intermediate phases such as Si–O–C may also form, which, if incompletely reacted, degrade the final material properties. In addition, cracks or nonuniform porosity may develop during gel drying due to sudden solvent evaporation, leading to reduced structural integrity. These issues highlight the necessity of precise control and optimization throughout the sol–gel process [17]. Figure 1 provides a schematic overview of the key sol–gel steps and resulting products.

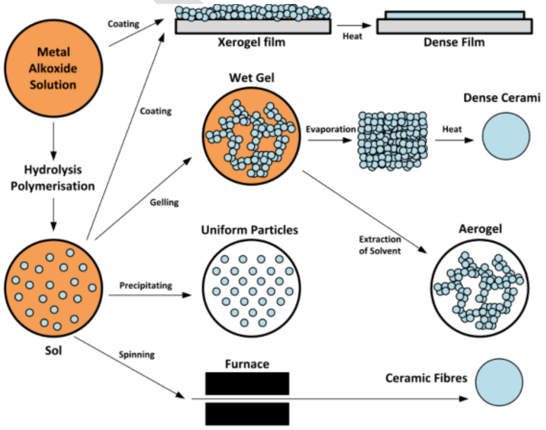

Figure 1: Schematic view of the sol-gel process [18].

This figure has inspired many visual representations of the sol-to-gel transition, and similar diagrams are frequently used in the literature to illustrate the sol–gel process [18]. As mentioned above, all previous methods required synthesis temperatures at least 50–250°C higher than in this

[DOI: 10.22068/ijmse.4346]

work and produced particles larger than 35 nm. Furthermore, none simultaneously achieved three critical goals: (i) controlled polytype synthesis (3C/6H), (ii) engineering of quantum vacancies (silicon-vacancy centers) for single-photon emission, and (iii) elimination of toxic chemicals. Despite previous reports on SiC nanomaterials with sizes ranging from micro- to nanoscale, precise control over nanostructure growth remains a critical challenge. In this research, we demonstrate a modified sol–gel method using TEOS and sucrose in an ethanol-based medium, with optimized calcination at 1350°C. This approach offers several unprecedented achievements: (i) reduction of the synthesis temperature to 1350°C, (ii) formation of SiC nanoparticles in the 15–30 nm range, (iii) generation of silicon-vacancy quantum centers with verified single-photon emission at 860 nm (confirmed by PL analysis); and (iv) complete elimination of hazardous corrosive chemicals such as HF, by employing an ethanol-based gel system, thereby reducing environmental risks and enhancing scalability.

2. Experimental

Ethanol (all supplied by Merck, Germany) was used as a precursor. The experimental steps are schematically illustrated in Figure 2. As can be seen, first a sol consisting of 2.2 ml of TEOS was prepared along with about 10 ml of ethanol, 0.5 ml of distilled water, and 2 g of sucrose. Then, hydrochloric acid was added as a catalyst in an amount of 2 mL to the solution. This solution was completely homogeneous and uniform for 3 hours by magnetic stirring.

[DOI: 10.22068/ijmse.4346]

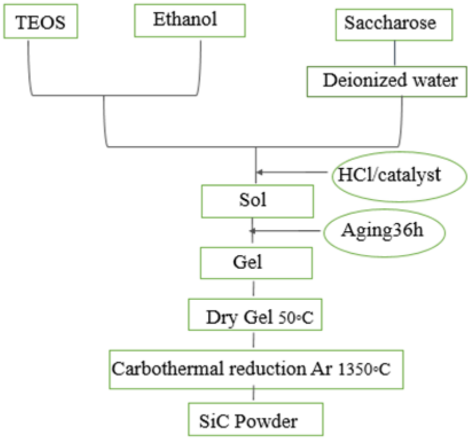

Figure 2: Schematic of the preparation of nanoparticles by the sol-gel method.

The resulting sol was transparent and colorless. The prepared sol was left to undergo gelation for 40 h at room temperature, after which it was dried at 50°C, yielding a dark brown powder. The obtained powder was then placed in an alumina crucible and subjected to heat treatment in a vacuum furnace under argon atmosphere at 1350°C for 3 h. The furnace chamber was initially evacuated to approximately 2×10^{-2} mbar. Argon gas was then introduced at a flow rate of about 100 sccm. After allowing the system to stabilize for approximately 10 minutes, the heating program began. The temperature was first raised to 1100 °C at a heating rate of 5 °C/min, and then increased from 1100 °C to 1350 °C at a controlled rate of 3 °C/min. For cooling, the furnace was switched off and allowed to return to room temperature naturally over several hours in ambient conditions. The final powder appeared dark in color. To characterize the synthesized powder, several analytical techniques were employed. The bonding types among the sample constituents were investigated using Fourier-transform infrared spectroscopy (FTIR) in the range of 400–4000 cm^{-1}. Phase identification and average crystallite size determination were performed via X-ray diffraction (XRD), employing the Debye–Scherrer method. For accurate grain size measurements, a Zeiss EM900 transmission electron microscope (TEM) was used. The morphology of the particles was examined using field-emission scanning electron microscopy (FESEM, Zeiss, model Sigma 30-HV). Photoluminescence (PL) spectra were recorded using excitation at 200 nm to

[DOI: 10.22068/ijmse.4346]

evaluate the optical emission characteristics of the synthesized SiC. Diffuse reflectance spectroscopy (DRS) was carried out with an Avantes Avaspec-2048 spectrometer in the range of 200–1100 nm. The Kubelka–Munk function was applied to convert the diffuse reflectance data for bandgap determination. Finally, Raman spectroscopy (Avantes, model uRaman-532-Ci) with a 532 nm laser in the range of 100–1400 cm^{-1} was employed to analyze lattice vibrations and confirm the crystalline structure of the synthesized SiC nanoparticles.

3. Result and Discussion

3.1 Structural study of silicon carbide nanoparticles

Initially, the X-ray diffraction spectrum of the resulting powder was taken. According to Figure 3, no peaks related to carbon gas or SiO_2 are observed in the sample, which indicates that the carbothermal reduction reaction is almost complete. The synthesized sample has peaks for 2Θ equal to 33.6, 35.8, 41.4, 60.04, 71.8 and 75.5 degrees. As shown in Figure 3, the 2θ values and the intensities of the main peaks at 35.6, 41.4 and 60.04° are in good agreement with the established values (JCPDS Card No. 29-1129) and can be attributed to the diffraction of the β-SiC (111), (200) and (220) planes, respectively [19]. The pronounced, sharp peaks indicate that the SiC nanoparticles exhibited good crystallinity. Therefore, β-SiC was confirmed as the primary crystalline phase of the nanosized particles with cubic structure. Also, the 2θ values and the main peaks at 33.6, 35.8, 71.8 and 75.5° degrees are in good agreement with the determined values (JCPDS card number 29-1131) and can be attributed to the diffraction of (101), (102), (116) and (0012) α-SiC planes, respectively, which indicates the presence of a hexagonal structure alongside the cubic structure. [20].

[DOI: 10.22068/ijmse.4346]

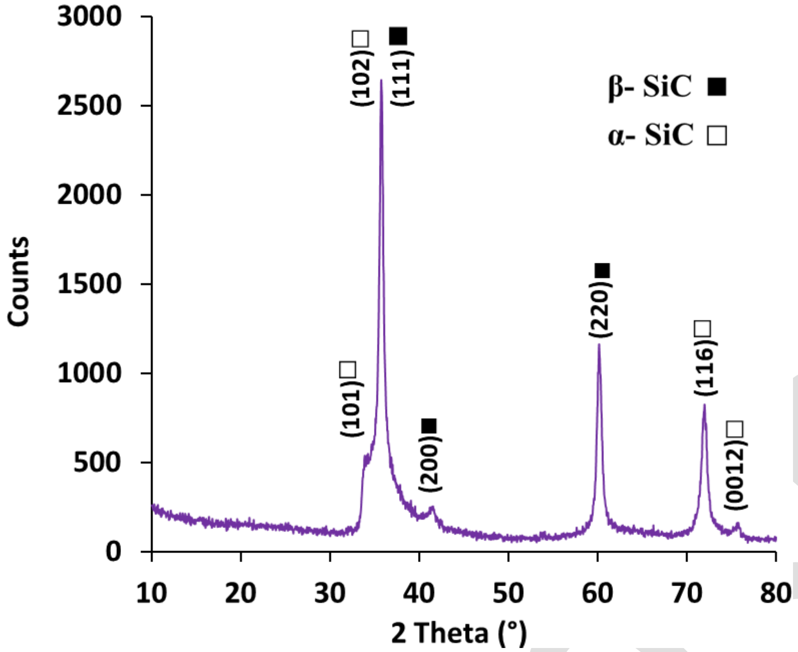

Figure 3: X-ray diffraction spectrum showing the formation of bi-structured *α-SiC* and *β-SiC* nanoparticles.

Using the X-ray diffraction spectrum and the Scherrer equation, the crystal dimensions can be determined as follows [21]:

$$D = (k\times\lambda) / (\mathrm{FWHM}\times\cos\theta) \qquad (1)$$

In this relation, D is the crystal size, k is the lattice constant (approximately 0.89), and λ is the wavelength of the incident beam, which is here the wavelength of the copper target and is considered to be 1.5406 angstroms. Also, θ is the diffraction angle, and FWHM shows the width at half maximum of the diffraction peak. Based on Scherrer's calculations, the crystal sizes were calculated for each of the phases in the sample and can be seen in Table 1.

Table 1: The determined average crystallite size of the sample obtained using X-ray diffraction spectrum.

Poly type	2Θ	FWHM	D	Average
β	35.6	0.508	~16 nm	~14 nm
	41.4	0.62	~14 nm	
	60.04	0.819	~12 nm	
α	35.6	0.508	~16 nm	~16 nm
	71.8	0.62	~14 nm	
	75.5	0.52	~19 nm	

[DOI: 10.22068/ijmse.4346]

Based on these calculations, the average crystal size was determined to be about 15 nm, which is a desirable result compared to the work of others and the expensive and even risky processes. The FTIR spectrum of the synthesized SiC nanoparticles is shown in Figure 4. An absorption peak was observed at 847 cm^{-1}, corresponding to the characteristic Si–C bond vibrations, formed by the bonding of carbon from sucrose with hydrolyzed silicon from TEOS at the molecular level. In addition, weak and broad absorption bands were detected in the 2300–3700 cm^{-1} region, which is almost certainly due to O-H stretching vibrations from adsorbed water [22].

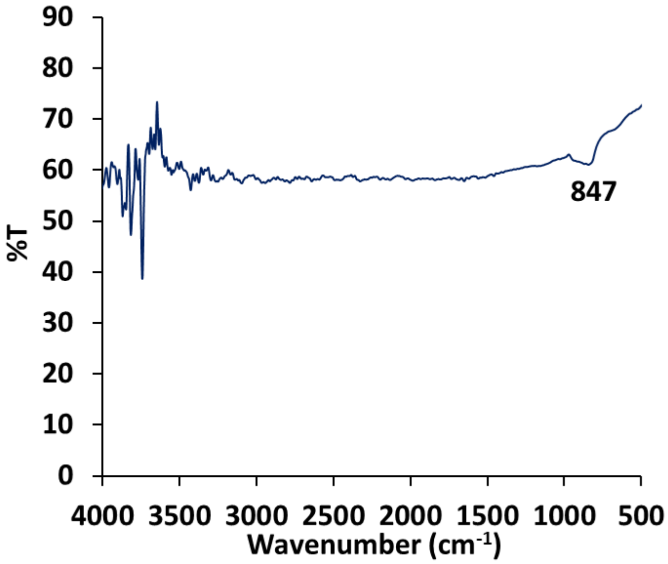

Figure 4: Infrared Fourier transform curve of silicon carbide nanoparticles.

Figure 5 shows the Raman spectrum of the synthesized powder. The presence of a characteristic peak around 782 cm^{-1} is observed, which is attributed to the transverse optical phonon (TO) mode in the cubic and hexagonal silicon carbide (6H-SiC, 3C-SiC) structure. This peak is known as a key feature for identifying the β-SiC and α-SiC phases and indicates the presence of both β and α phases in the sample structure. In addition, a peak appears in the range of 930–970 cm^{-1}, which is related to the longitudinal optical phonon (LO) mode and can be present in both 3C and 6H structures, which is in good agreement with the XRD analysis data. In the higher wavenumber regions (1330–1510 cm^{-1}), peaks are also observed that are attributed to second-order Raman

[DOI: 10.22068/ijmse.4346]

processes such as TO or TO+LO combinations and are usually observed in structures where free or amorphous carbon is present. The presence of these strong and distinct peaks in the Raman spectrum indicates the desirable crystallinity and high quality of the synthesized nanoparticles [23].

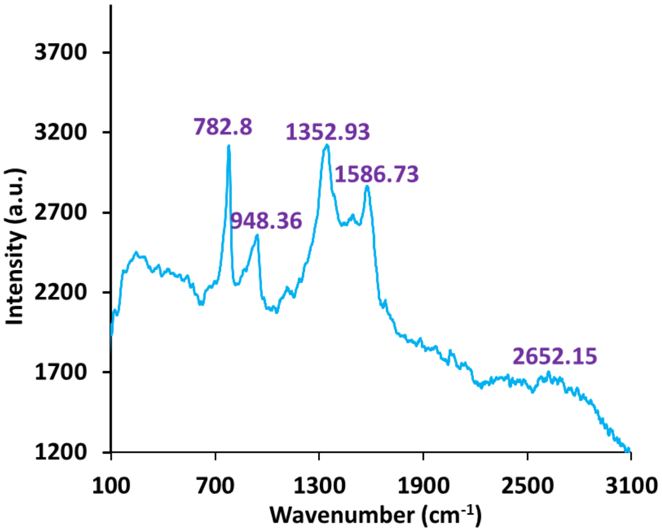

Figure 5: Raman curve of synthesized silicon carbide nanoparticles.

As shown in Figure 6, the morphology and structure of the synthesized SiC nanoparticles were studied using FESEM and TEM techniques. The TEM image in Figure 6(a) is a dark field image with (111) orientation of the selected area of the sample. The SEM images in Figures 6(b) and 6(c) show the formation of regular and spherical SiC nanoparticles. As can be seen, the synthesized nanoparticles have a relatively uniform size distribution in the range of 30–40 nm [24]. Figure 6(c) shows the EDX spectrum of the synthesized silicon carbide nanoparticles. As can be seen from the percentage of elements, in addition to the formation of silicon carbide, a large amount of carbon atoms are present in the sample, which confirms the presence of free carbons at 1330 and 1510 in the Raman diagram (Figure 5) [25]. The low percentage of oxygen (O) could be due to surface oxygen adsorption or the formation of a thin surface oxide layer, which significantly reduces the possibility of SiO_2 bond formation, and XRD (Figure 3) and Raman (Figure 5) analyses also confirm the lack of SiO_2 formation.

[DOI: 10.22068/ijmse.4346]

[DOI: 10.22068/ijmse.4346]

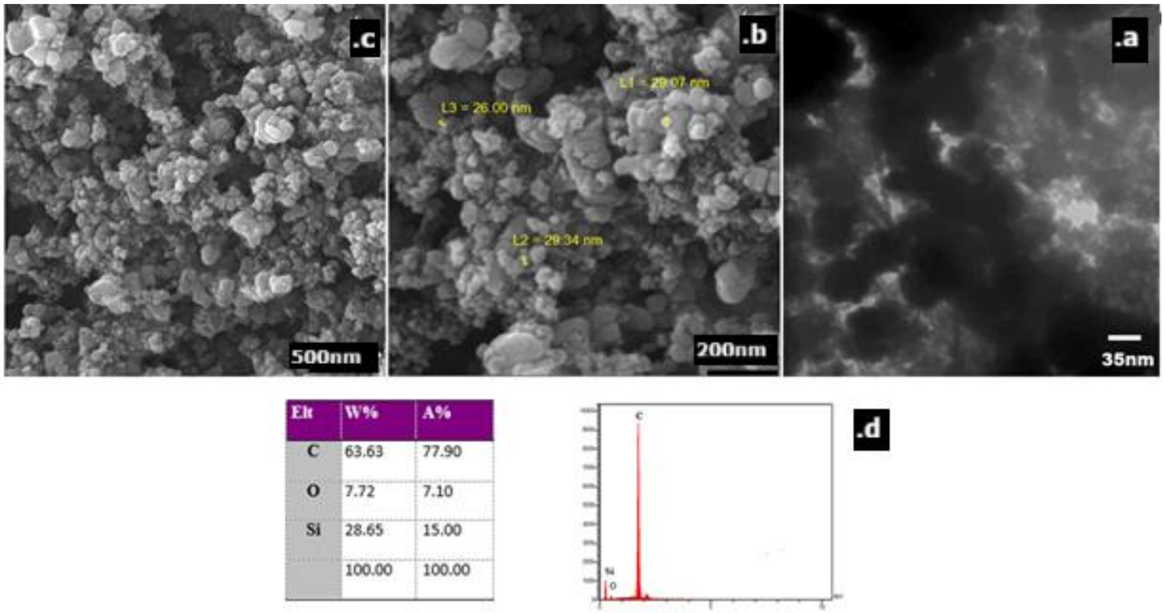

Elt	W%	A%
C	63.63	77.90
O	7.72	7.10
Si	28.65	15.00
	100.00	100.00

Figure 6: a) TEM , b) and c) FESEM images , d) EDX of silicon carbide nanoparticles.

3.2 Optical study of silicon carbide nanoparticles

To investigate the optical properties, the synthesized sample was subjected to photoluminescence spectroscopy with an excitation wavelength of 200 nm (Figure 7). As can be seen in this figure, there are distinct peaks in the UV-Vis and IR regions, each of which is related to different mechanisms of radiative recombination and atomic vacancies. The intense peaks at 400 and 600 nm are related to the first and second harmonics of the excitation wavelength. The sharp peak observed at about 361 nm is located in the ultraviolet region and is attributed to band-edge recombination in the synthesized sample structure. In the 4H-SiC structure, the indirect energy gap of about 3.3 eV corresponds to a wavelength of approximately 375 nm. The slight shift of this peak towards shorter wavelength (361 nm) indicates the quantum confinement effect in the nanoparticles, which causes an increase in the band gap. Therefore, this emission is mainly related to the α-SiC phase and is modified by the small particle size [26]. The peak observed at 461 nm is located in the visible-blue region and is related to the emission due to lattice defects. Stacking faults and layer discontinuities in hexagonal polytypes (α-SiC) can produce such optical emissions in the visible region. Hence, this peak is also attributed to structural defects in α-SiC [27]. The peak observed at around 731 nm is due to the donor-acceptor transitions in the β (3C-SiC) structure. These transitions are the result of the recombination of electrons trapped in the donor levels with holes in the acceptor levels within the energy gap, which are often due to intrinsic lattice defects such as silicon or carbon vacancies. The presence of this peak in the PL spectrum indicates that part of the sample is formed as a cubic polytype (β-SiC), and structural defects in this phase play an effective role in generating red emission [28]. In the near-infrared region, peaks appear at around 820, 829, and 872 nm. These peaks, which are due to silicon vacancies (VSi) and zero-phonon lines (ZPL) of the V1 center in 4H-SiC, are located. The shift of these peaks towards shorter wavelengths can be due to electron-phonon interactions. Therefore, these emissions are directly related to VSi centers in the α phase, (4H-SiC). In general, the PL spectrum shows that both α and β phases are present in the synthesized nanoparticles. Still, the presence of the α phase dominates over the β phase, as indicated by structural analyses. The IR emissions, which are mainly due to vacancy centers, are of particular importance for applications in quantum technologies and biosensors [29-32].

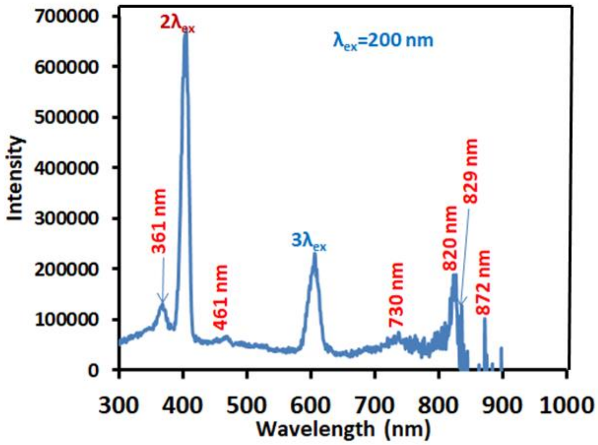

Figure 7: PL spectrum of silicon carbide nanoparticles with 200 nm excitation.

[DOI: 10.22068/ijmse.4346]

n the ultraviolet-visible region was also used. Given the powdery nature and nanoscale structure of the sample, the use of the direct UV–Vis absorption method could have resulted in unrealistic data due to the intense light scattering. For this reason, to eliminate the scattering effects, the diffuse reflectance was transformed into the Kubelka–Munk function, which is defined as $F(R)=(1-R)^2/2R$, where R is the relative reflectance. To determine the band gap energy, the Tauke relation for semiconductors with an indirect band gap and a dependence on the power of one square was used. In this method, the $(F(R)\cdot E)^{1/2}$ plot was plotted in terms of photon energy, and the band gap energy (E_g) was determined by extrapolating the linear part of the curve to the horizontal axis (Figure 8). The band gap energy obtained for the sample is about 3.2 eV, which corresponds to a wavelength of about 388 nm and is in relative agreement with the values reported for the β-SiC and α-SiC phases [33,34]. This value shows a slight increase compared to the band gap of the cubic face-packed structure, which can be attributed to the quantum confinement caused by the reduction in crystal size. When the crystal dimensions are reduced below the Bohr radius of the exciton, the electronic structure of the material changes, and the band gap increases. On the other hand, the relatively high synthesis temperature (1350°C) provides the conditions for the formation of a stable hexagonal (4H/6H)-SiC phase of silicon carbide alongside 3C-SiC without leading to significant grain growth. Overall, DRS results show that both α and β phases are present in the sample, but the dominant band gap measured is due to the α (4H/6H)-SiC phase. This finding is also consistent with the PL spectroscopy results, confirming that the observed band-edge emission in the ultraviolet region is mainly attributed to the α-SiC structure. This indicates that the preservation of nanoscale dimensions, along with the desired crystallinity of the material, plays an important role in tuning its optical properties [35].

[DOI: 10.22068/ijmse.4346]

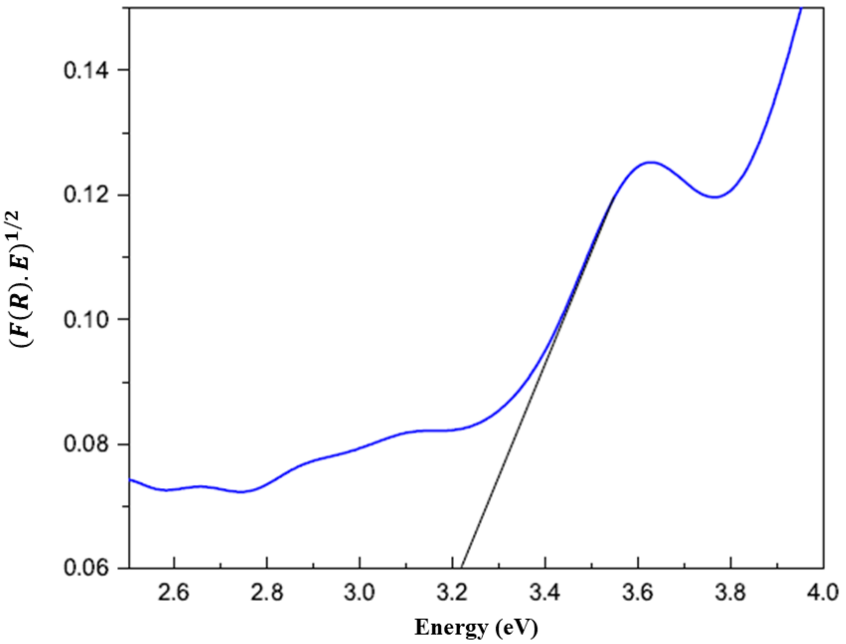

Figure 8: DRS spectrum of silicon carbide nanoparticles for band gap determination.

3.3 Comparison of the results obtained with the work of others

Table 2, compares the results obtained from this study with the results of other researchers.

Table 2: Comparison of recent studies with the present work.

Study (Year)	Synthesis Method	Temperature (°C)	Particle Size (nm)	Limitations
Najafi et al. (2022) [11]	Acid-catalyzed sol–gel	1500	~50	Requirement of HF, lack of polytype control
Li et al. (2023) [12]	Sol–gel + catalyst	1550	~60	Mixed phases
Garcia et al. (2019) [14]	Plasma pyrolysis	1700	>200	High equipment cost
Chen et al. (2021) [15]	Carbothermal + MA	1550	>100	High energy consumption
Wang et al. (2022) [16]	CVD	1580	100–300	Toxic precursors
Patel et al. (2023) [36]	Fe-assisted sol–gel	1520	~35	Iron contamination
This work	Modified sol–gel	1350	15–30	----------------------

As shown in Table 2, all previous methods have a temperature of at least 100 to 250 °C higher than this study, and the particle size is more than 35 nm. In addition, none of them have simultaneously achieved the three goals of controlling the 3C/6H polytype, nanosized particles preparation with

[DOI: 10.22068/ijmse.4346]

silicon vacancies, and removing toxic materials. Despite the synthesis of SiC nanomaterials with dimensions ranging from micrometers to nanometers by various methods, controlling the growth of SiC nanostructures remains a significant challenge in the development of nanotechnology. In this study, by using a modified sol-gel method based on tetraethyl orthosilicate and sucrose in an ethanolic environment and optimizing the calcination conditions of 1350°C, we have achieved desirable results: Reducing the synthesis temperature to 1350°C, lower than all the studies compared in Table 2, forming SiC nanoparticles (with a size of 20-30 nm), the smallest size reported in similar methods, creating Si vacancy quantum dots with single-photon emission at 872 nm confirmed by (PL) and complete removal of toxic corrosive materials such as (HF) and using an ethanol-based gelation system, to reduce environmental risk and increase scalability.

1. Conclusion

In this study, silicon carbide nanoparticles were successfully synthesized by the sol-gel method and carbothermal reduction at 1350°C. XRD and Raman results revealed the simultaneous presence of both α and β polytypes and showed a favorable crystallinity pattern. FESEM and TEM images showed that the synthesized particles had a uniform morphology and a size of about 30-40 nm. DRS analysis showed a band gap of about 3.2 eV, which was in perfect agreement with the band edge peak in PL. Also, the PL spectrum revealed peaks related to lattice defects and vacancy centers in addition to the band edge emission, which, along with structural data, helps to provide a deeper understanding of the phase composition and optical nature of the sample. The overlap of the results of different analyses indicates that the synthesis process performed was reliable and the final product was of high purity and quality. On the other hand, the observed optical and structural properties indicate the broad capabilities of the synthesized SiC nanoparticles for application in advanced fields such as quantum technology.

5. Reference

[1] Capan, I., "*Defects in Silicon Carbide as Quantum Qubits: Recent Advances in Defect Engineering*." *Appl. Sci.*, 2025, 15, 5606.

[2] Castelletto, S., Johnson, B. C., Ivády, V., Stavrias, N., Umeda, T., Gali, A. and Ohshima, T., "*A Silicon Carbide Room-Temperature Single-Photon Source*." *Nat. Mater.*, 2014, 13, 151–156.

[3] Radulaski, M., Widmann, M., Niethammer, M., Zhang, J. L., Lee, S. Y., Rendler, T. and Vuckovic, J., "*Scalable Quantum Photonics with Single Color Centers in Silicon Carbide.*" *Nano Lett.*, 2017, 17, 1782–1786.

[4] Soltys, L. M., Mironyuk, I. F., Mykytyn, I. M., Hnylytsia, I. D. and Turovska, L. V., "*Synthesis and Properties of Silicon Carbide.*" *Phys. Chem. Solid State*, 2023, 24, 5–16.

[5] Seo, W. S. and Koumoto, K., "*Stacking-Fault-Induced Fracture in SiC Particles Synthesized by Carbothermal Reduction.*" *J. Am. Ceram. Soc.*, 1996, 79, 1777–1784.

[6] Li, Y. L., Qiao, G. J. and Jin, Z. H., "*CVD Growth of β-SiC Films on Si (100) Substrates Using Hexamethyldisilane.*" *Mater. Lett.*, 2002, 54, 76–80.

[7] Shimoo, T., Takeuchi, H. and Okamura, K., "*Synthesis of Ultrafine β-SiC Powder by Direct Carbonization of Silicon Metal.*" *J. Mater. Sci.*, 2000, 35, 3301–3306.

[8] Zhang, L. and Koc, R., "*Ultrafine Silicon Carbide Powders Synthesis by Mechanical Alloying.*" *J. Mater. Sci.*, 2017, 52, 2847–2858.

[9] Wang, H., Li, Y., Zhang, G. and Li, H., "*Removal of Surface Oxide and Its Effect on the Synthesis of SiC Nanoparticles via Carbothermal Reduction.*" *Ceram. Int.*, 2015, 41, 14511–14517.

[10] Brinker, C. J. and Scherer, G. W., *Sol-Gel Science: The Physics and Chemistry of Sol-Gel Processing*, Academic Press, San Diego, CA, USA, 1990.

[11] Najafi, A., Moghaddam, M. S. and Faghihi-Sani, M. A., "*Acid-Catalyzed Sol-Gel Synthesis of β-SiC Nanoparticles: Effect of pH on Particle Size and Phase Purity*." *J. Eur. Ceram. Soc.*, 2022, 42, 3620–3627.

[12] Li, X., Wang, Y., Chen, Z. and Zhang, Q., "*Dual-Catalyst Assisted Sol-Gel Synthesis of 60 nm SiC Nanoparticles at 1500°C.*" *Mater. Chem. Phys.*, 2023, 301, 127642.

[13] Zhang, Y., Li, J. and Shen, Z., "*Low-Temperature Synthesis of β-SiC Nanoparticles via Carbon–Silica Mixture Route*." *J. Alloys Compd.*, 2020, 832, 154955.

[14] Garcia, E. V., Lopez-Honorato, E. and Meadows, P. J., “Plasma Pyrolysis Synthesis of SiC Micro-Powders at 1700°C.” *Ceram. Int.*, 2019, 45, 17378–17385.

[DOI: 10.22068/ijmse.4346]

[15] Chen, R., Xu, L. and Liu, B., "*Mechanically Activated Carbothermal Synthesis of SiC Powders at 1550°C.*" *Powder Technol.*, 2021, 380, 585–592.

[16] Wang, T. and Li, H., "*High-Temperature CVD Growth of SiC Microstructures at 1580°C.*" *Thin Solid Films*, 2022, 744, 139078.

[17] Jones, R. and Rabel, A. M., "*Challenges in Sol-Gel Synthesis of Silicon Carbide Ceramics: Phase Purity and Particle Growth*." *J. Sol-Gel Sci. Technol.*, 2018, 87, 432–443.

[18] "Sol-Gel Technology Stages", Wikimedia Commons, https://en.wikipedia.org/wiki/File:SolGelTechnologyStages.svg

[19] Wang, B., Shang, X., Zhang, J., Shen, J., Wang, X. and Zhang, Z., "*Crystal Phase Engineering SiC Nanosheets for Enhancing Photocatalytic CO_2 Reduction*." *Environ. Sci. Adv.*, 2023, 2, 132–139.

[20] Feller, T., Rosenfeldt, S. and Retsch, M., "*Carbothermal Synthesis of Micron-Sized, Uniform, Spherical Silicon Carbide (SiC) Particles*." *Z. Anorg. Allg. Chem.*, 2021, 647, 2172–2180.

[21] Solgi, S., Sasani Ghamsari, M., Tafreshi, M. J. and Karvane, R., "*Synthesis Condition Effects on the Emission Enhancement of YBO_3 Powder.*" *Optik*, 2020, 218, 165031.

[22] Sanz, N., Boudet, A. and Ibanez, A., "*Melting Behavior of Organic Nanocrystals Grown in Sol–Gel Matrices*." *J. Nanopart. Res.*, 2002, 4, 99–105.

[23] Nakashima, S. and Harima, H., "*Raman Investigation of SiC Polytypes*." *Phys. Status Solidi A*, 1997, 162, 39–64.

[24] Williams, D. B. and Carter, C. B., "Transmission Electron Microscopy," *Systematic Materials Analysis*, ed. J. H. Richardson and R. V. Peterson, Academic Press, New York, USA, 1978, 4, 407–432.

[25] Potgieter-Vermaak, S., Maledi, N., Wagner, N., Van Heerden, J. H. P., Van Grieken, R. and Potgieter, J. H., "*Raman Spectroscopy for the Analysis of Coal: A Review*." *J. Raman Spectrosc.*, 2011, 42, 123–129.

[26] Zhen, C. M., Zhang, J. J., Wang, X. Q., Zhang, Y. J., Pan, C. F. and Hou, D. L., "*Investigation of Luminescence from SiC Nano-Granule Films on Porous Glass Substrate*." *Optoelectron. Lett.*, 2008, 4, 429–432.

[27] Vasquez, G. C., Bathen, M. E., Galeckas, A., Bazioti, C., Johansen, K. M., Maestre, D. and Vines, L., "*Strain Modulation of Si Vacancy Emission from SiC Micro- and Nanoparticles*." *Nano Lett.*, 2020, 20, 8689–8695.

[28] Sun, J. W., Jokubavicius, V., Gao, L., Booker, I., Jansson, M., Liu, X. Y. and Syväjärvi, M., "*Solar Driven Energy Conversion Applications Based on 3C-SiC.*" *Mater. Sci. Forum*, 2016, 858, 1028–1031.

[DOI: 10.22068/ijmse.4346]

[29] Bathen, M. E., Galeckas, A., Karsthof, R., Delteil, A., Sallet, V., Kuznetsov, A. Y. and Vines, L., "*Resolving Jahn–Teller Induced Vibronic Fine Structure of Silicon Vacancy Quantum Emission in Silicon Carbide*." *Phys. Rev. B*, 2021, 104, 045120.

[30] Hasanzadeh Azar, M., Jahanzamin, J., Ji, Z., Kitai, A., Beke, D. and Gali, A., "*Recent Advances in the Synthesis, Optical Properties, and Applications of Fluorescent Silicon Carbide Quantum Dots*." *Small Sci.*, 2025, 2500013.

[31] De Vries, M. O., Sato, S. I., Ohshima, T., Gibson, B. C., Bluet, J. M., Castelletto, S. and Reineck, P., "*Fluorescent Silicon Carbide Nanoparticles*." *Adv. Opt. Mater.*, 2021, 9, 2100311.

[32] Luo, Q. Y., Li, Q., Wang, J. F., Guo, P. J., Lin, W. X., Zhao, S. and Guo, G. C., "Fabrication and Quantum Sensing of Spin Defects in Silicon Carbide." *Front. Phys.*, 2023, 11, 1270602.

[33] Krambrock, K. and Spaeth, J. M., "*Optical Absorption of the Cubic and Hexagonal SiC Polytypes*." *J. Phys. Condens. Matter*, 1999, 11, L543.

[34] Wellenhoff, G. and Spencer, M. G., "*Bandgap Determination of 3C-SiC and 6H-SiC by Diffuse Reflectance Spectroscopy*." *J. Appl. Phys.*, 1998, 84, 2920–2923.

[35] Efros, A. L. and Rosen, M., "*The Electronic Structure of Semiconductor Nanocrystals*." *Annu. Rev. Mater. Sci.*, 2000, 30, 475–521.

[36] Patel, S., Kumar, R. and Gupta, M., "*Iron-Assisted Sol-Gel Synthesis of 35 nm SiC Powders at 1520°C.*" *Mater. Lett.*, 2023, 331, 133476.

[DOI: 10.22068/ijmse.4346]